AGU PUBLICATIONS

Journal of Advances in Modeling Earth Systems

RESEARCH ARTICLE
10.1002/2016MS000901

Sensitivity of transpiration to subsurface properties: Exploration with a 1-D model

Michail D. Vrettas[1,2] and Inez Y. Fung[1]

[1]Department of Earth and Planetary Science, University of California, Berkeley, California, USA, [2]Now at Central Laser Facility, Rutherford Appleton Laboratory, Harwell Campus, Oxford, UK

Key Points:
- In a Mediterranean climate, weathered bedrock is a reservoir that sustains evapotranspiration (ET) of deep-rooted trees in the dry season
- The magnitude of annual ET depends on lithology, tree species, rooting depths and capability for hydraulic redistribution
- A small feedback exists in the root zone, where ET depletion of moisture decreases hydraulic conductivity and enhances moisture retention

Correspondence to:
I. Fung,
ifung@berkeley.edu

Citation:
Vrettas, M. D., and I. Y. Fung (2017), Sensitivity of transpiration to subsurface properties: Exploration with a 1-D model, *J. Adv. Model. Earth Syst.*, *9*, 1030–1045, doi:10.1002/2016MS000901.

Received 20 DEC 2016
Accepted 7 APR 2017
Accepted article online 14 APR 2017
Published online 4 MAY 2017

Abstract The amount of moisture transpired by vegetation is critically tied to the moisture supply accessible to the root zone. In a Mediterranean climate, integrated evapotranspiration (ET) is typically greater in the dry summer when there is an uninterrupted period of high insolation. We present a 1-D model to explore the subsurface factors that may sustain ET through the dry season. The model includes a stochastic parameterization of hydraulic conductivity, root water uptake efficiency, and hydraulic redistribution by plant roots. Model experiments vary the precipitation, the magnitude and seasonality of ET demand, as well as rooting profiles and rooting depths of the vegetation. The results show that the amount of subsurface moisture remaining at the end of the wet winter is determined by the competition among abundant precipitation input, fast infiltration, and winter ET demand. The weathered bedrock retains ~30% of the winter rain and provides a substantial moisture reservoir that may sustain ET of deep-rooted (>8 m) trees through the dry season. A small negative feedback exists in the root zone, where the depletion of moisture by ET decreases hydraulic conductivity and enhances the retention of moisture. Hence, hydraulic redistribution by plant roots is impactful in a dry season, or with a less conductive subsurface. Suggestions for implementing the model in the CESM are discussed.

1. Introduction

Climate change is projected to alter both the means, as well as extremes, of temperature and precipitation [*Kharin et al.*, 2013; *Sillmann et al.*, 2013a,b; *Scoccimarro et al.*, 2013]. At a given location, even if the annual mean precipitation remains at the current level, the timing and intensity of precipitation events will change. Precipitation, when it occurs, will likely be more intense, and droughts will likely be prolonged. The changing hydrologic regimes have important implications for ecosystem survival and freshwater availability, as well as for the carbon cycle and climate. This is illustrated by the wide range in the magnitude of the feedbacks between land carbon dynamics and climate in the Earth System Models participating in the Intergovernmental Panel on Climate Change (IPCC) Coupled Carbon Cycle Climate Model Intercomparison Project (C4MIP) [*Friedlingstein et al.*, 2006; *Arora et al.*, 2013].

While all the C4MIP models in the IPCC 4th Assessment Report projected a drying of the tropics and an enhancement of evaporation with warming, the degree of soil moisture decrease varied substantially among the models. The Amazonian rainforest collapsed in one model and led to a massive release of CO_2 to the atmosphere [*Cox et al.*, 2000], while in another model the decrease in photosynthesis had only a small impact on atmospheric CO_2 and climate [*Fung et al.*, 2005]. In another climate model experiment, the depletion of soil moisture resulting from large-scale midlatitude afforestation led to large-scale warming of the northern hemisphere and a shift of the Intertropical Convergence Zone (ITCZ) [*Swann et al.*, 2012].

With precipitation events, whether water will infiltrate to the subsurface and be stored or will contribute to surface runoff and streamflow depends not only on precipitation intensity and topography but also on subsurface lithology and dynamics. Additionally, whether water in the subsurface will be concentrated near the surface and become available for evaporation or be distributed through a greater depth to sustain plants through the dry season may impact ecosystem function and climate. For example, after the European heat wave of 2003 forests initially heated up faster than grasslands but did not reach the high temperatures of the grasslands, whose shallow roots quickly depleted the near-surface pool of soil moisture for evapotranspiration. Thereafter, the net radiation of the grasslands was balanced by sensible heating [*Teuling et al.*,

2010]. Hyperspectral observations show nonuniform loss of canopy water across California during the prolonged drought 2011–2015 [*Asner et al*., 2016]. In a review, *van der Molen et al*. [2011] showed that drought impacts on the carbon cycle persist months to years after a drought, termed *carry over effect*, due to soil memory, and argue that plant strategies must be a key component in Dynamic Global Vegetation Models (DGVMs).

For the same climate and environmental conditions, plant investment in shallow roots has competitive advantages over investment in deep roots [*Schenk*, 2008; *Poot and Lambers*, 2008]. However, for water-limited ecosystems, a strategy for optimal water use may include deep roots [e.g., *Collins and Bras*, 2007; *Schenk and Jackson*, 2002a] and/or roots in rocks [*Schwinning*, 2010]. Deep roots and deep moisture reservoirs may be synergistic, as fractures or fissures in weathered bedrock below the soil mantle could facilitate both the storage of water and the development of roots. The growth of roots expands the "macropores" and the decay of roots leaves behind preferential flow conduits. There is a growing body of work that describes roots that extend to great depths and roots in rocks that access deep moisture reservoirs [e.g., *Zwieniecki and Newton*, 1996; *Schwinning*, 2010]. For example, in the Eastern Amazon 3/4 of the water transpired is extracted by roots located 2−8 m below the surface [*Nepstad et al*., 1994]. *Jackson et al*. [1999] found that, in *Powell's cave* in Texas, evergreen oaks have maximum rooting depth of 25 m and take up water from 18 m depth as a strategy for growth and survival.

Plant root distributions and functions are adapted to optimize the use of available resources. In addition to development of deep roots in water-limited regions or regions with water resources at depth, another strategy is hydraulic redistribution (HR), wherein there is rapid downward transfer of water by the tap roots after rains or at night, and upward transfer of water to the fine roots during the day [*Dawson*, 1993; *Oliveira et al*., 2005]. Hydraulic redistribution is found in over 60 species, and exceptions are found in only 3 tree species and 1 grass species. The implementation of hydraulic redistribution in global and regional climate models has been shown to enhance transpiration in the dry season (defined by precipitation) and impact regional climate [*Lee et al*., 2006; *Leung et al*., 2011; *Tang et al*., 2015].

Storage of water at depth requires transport into regions with low porosity. Subsurface water transport in conventional Earth Systems Models is typically represented by flow in a porous matrix, described using approximations to or simplification of the Richards' and Darcy flow equations [*Oleson et al*., 2013; *Lawrence et al*., 2011]. For over 30 years, however, hydrologists have recognized that pore-scale flow processes may provide only a secondary control on water transport within hillslopes, with the majority of water transport being associated with relatively fast flow through fractures or macropores, i.e., preferential flow [*Beven and Germann*, 2013].

Models developed for flow in porous media are inadequate for representing systems dominated by preferential flow. Reproducing the rapid flux of water from preferentially drained hillslopes to runoff with Richards' equation requires artificially boosting the hydraulic conductivity of soils, leading to an underestimation of near-surface water, with consequences for evapotranspiration. Preserving the correct near-surface soil moisture dynamics, however, underestimates infiltration and subsequently the runoff. Indeed, *Band et al*. [2014], recognizing the importance of preferential flow in subsurface networks in water transport, calls for a community effort to design and implement a set of well-planned experiments in different natural and constructed hillslopes, coupled with the development of new theory and methods to explicitly incorporate and couple the coevolution of subsurface flow networks as intrinsic components of hydrological, ecological, and geomorphic systems.

The current study is motivated by the multiyear, high-frequency observations of water table depth, precipitation, and sapflow velocities, taken at a research site dubbed "Rivendell": a steep (35°), small (∼4000 m^2) watershed in the Angelo Coast Range Reserve within the Eel River watershed in Northern California. The climate is Mediterranean, with an average annual precipitation of ∼1800 mm/a, ∼80% of which falls between October and March. A "water year" (WY) refers to the period from 1 October to 30 September of the following year.

The hillslope at Rivendell is made up of a thin soil mantle of mixed organic and mineral matter overlying a bedrock whose thin upper saprolite layer of very broken and degraded rocks is on top of a thick partially weathered layer with fractures and macropores. The water tables, some 20−25 m below the surface, can rise by 1 m or more within hours after the first winter storms, and slowly decline [*Salve et al*., 2012]. The old-

growth forest is evergreen, comprising Douglas-fir (*Pseudotsuga menziesii*), coast redwood (*Sequoia sempervirens*), interior live oak (*Quercus wislizeni*), tanoak (*Notholithocarpus densiflorus*), Pacific madrones (*Arbutus menziesii*), and California bay (*Umbellularia californica*), without the presence of dense ground cover. Four years of high-frequency (less than 30 min) measurements of sapflow velocities show that these trees exhibit very different behaviors, with sapflow velocities peaking in the wet winter for Douglas-firs, and in the dry summer for Pacific madrones. At the same location, *Link et al*. [2014] derived analytic expressions that describe, for each tree species, the relationship of daily normalized sapflow velocities to solar irradiance, vapor pressure deficit (VPD), and near-surface soil moisture. The available observations are inadequate, however, to yield insight into the subsurface distribution of moisture, especially how trees access the moisture for transpiration during the dry summers.

This work advances a model for exploring the sensitivity of transpiration to subsurface water storage, rooting depth, and root functioning. It builds on *Vrettas and Fung* [2015], which presents a new stochastic parameterization for hydraulic conductivity that captures the rapid fluctuations of the water table at seven wells over a 6 years period at "Rivendell." This rapid rise and slow decline of the water table is not unique to the specific research site, but is observed in multiple wells across the US, and cannot be captured by the existing parameterization in, for example, the Community Land Model CLM [*Oleson et al*., 2013]. In a series of sensitivity experiments, we specify ET demands by different tree species by their annual magnitude and seasonality, and we ask what subsurface properties are needed to meet the ET demands. The results could thus be interpreted in terms of what root distributions and functions are required for survival in this climate and geologic setting.

The organization of the rest of the paper is as follows: Section 2 describes the 1-D model that is used to simulate the water flow in the vadose zone. A more detailed presentation of this model is given in *Vrettas and Fung* [2015], since here we extend this approach by including other processes such as evapotranspiration and hydraulic redistribution, which are described in section 3. The setup of the experimental part is given in section 4, with section 5 providing our findings. The paper concludes with a summary of this work, including a discussion, in section 6.

2. Model

Following the work of *Vrettas and Fung* [2015], this article considers a 1-D (vertical) column comprising a thin (0.5 m deep) soil mantle on top of a saprolite (1.5 m deep) and a weathered bedrock layer, overlying the continuously saturated bedrock with minimal permeability located at a depth of 20 m.

The equation governing the flow in the vadose zone is a modified Richards' PDE, which in its matric potential form is given by

$$\mathrm{C}\cdot\frac{\partial\psi}{\partial t}=\frac{\partial}{\partial z}\left[\mathrm{K}\cdot\left(\frac{\partial\psi}{\partial z}-1\right)-\mathrm{HR}\right]+\mathrm{P}-\mathrm{ET}-\mathrm{LF}, \tag{1}$$

with "z" and "t" the spatial [L: cm] (vertical coordinate-positive downward) and temporal [T: h] dimensions, respectively. Here $\psi(z,t)$ [L] is the matric potential (i.e., pressure head), with C representing the specific moisture capacity [1/L], that describes the rate of change in soil moisture θ with respect to the change in matric potential (i.e., $d\theta/d\psi$), while K is the (unsaturated) hydraulic conductivity [L/T]. The additional terms HR, P, LF, and ET correspond to the hydraulic redistribution, precipitation input, lateral (subsurface) flow, and evapotranspiration, respectively, and are described in the following sections.

Precipitation input (P) in equation (1) is throughfall or water that reaches the soil surface and enters the spatial domain, assuming no other losses. We set the canopy interception at 10% of the annual precipitation (of each simulated water year), a value typical of broadleaved evergreen forests [*Miralles et al*., 2010], and that amount is removed uniformly throughout the whole period.

The relationship between the matric potential $\psi(z,t)$ and the volumetric water content $\theta(z,t)$ [$\mathrm{L}^3/\mathrm{L}^3$], in equation (1), is not unique and several forms have been proposed. Among the most widely used are those of *Gardner* [1957], *Brooks and Corey* [1964], as well as *van Genuchten* [1980]. In this work the latter choice was implemented because it better models soils near and at full saturation [*van Genuchten and Nielsen*, 1985]. This is given by the nonlinear mapping as

$$\theta(\psi)=\theta_{res}+(\theta_{sat}(z)-\theta_{res})\cdot(1+(\alpha|\psi|)^{n})^{-m}, \quad (2)$$

with parameters $\alpha=0.009$ [1/L], $n=2$, $m=0.5$, the minimum (residual) water content is set to $\theta_{res}=0.04$ and $\theta_{sat}(z)$ is a porosity function that decays exponentially with depth "z" ranging in $[0.04,\ 0.30]$.

2.1. Boundary Conditions

Equation (1) is solved numerically for the pressure head variable $\psi(z,t)$, after discretizing the spatial domain "z" with a small step (e.g., $\Delta z=5$ cm), with appropriate initial and boundary conditions. It is understood that such a fine discretization would not scale efficiently at a global scale, but in this work it helps with monitoring the fast fluctuations of the observed water table in the underground with greater accuracy, and allows us to compute an estimate of the lateral subsurface flow. The discretization can readily be altered for a different setting.

Precipitation is measured continuously and binned at 30 min time intervals. Since we assume that a portion of this value is intercepted by vegetation and never reaches the soil (interception is set to 10%), we shall use P(t) to be equal to 90% of actual precipitation. It is used here as flux boundary condition (Neumann-type), at the ground surface, as

$$(\mathrm{K}(\psi)\cdot(\psi_z-1)-\mathrm{HR}(\psi,z))|_{z=0}=\mathrm{P}(t)\,, \quad \text{for } t\geq 0\,, \quad (3)$$

where now the dependencies of each parameter with "z," "t," and ψ, have been made explicit. We emphasize that at the site of our investigation the precipitation that reaches the surface is not sufficient to produce ponding or surface runoff that could introduce a change to the boundary condition. Therefore, such processes are omitted.

At the bottom of the domain, taken to be 20 m, a similar type condition is applied, with no water draining downward (zero flux), as the saturated hydraulic conductivity of the fresh bedrock layer is orders of magnitude smaller, compared to the upper layers. Therefore,

$$\mathrm{K}(\psi)\cdot(\psi_z-1)|_{z=20}=0\,, \quad \text{for } t\geq 0\,. \quad (4)$$

Note here that the $\mathrm{HR}(\psi,z)$ is not included in the bottom boundary condition, simply because the hydraulic redistribution process in our simulations does not reach the full depth of the vertical domain.

2.2. Hydraulic Conductivity

In *Vrettas and Fung* [2015], a new stochastic parameterization of hydraulic conductivity was introduced to capture the rapid flow of the water through fractures and preferential pathways in the weathered bedrock. In this new approach K is equal to the product of the normalized water content Θ and a stochastic background process $\mathrm{K_{bkg}}$, drawn from a lognormal distribution as follows:

$$\mathrm{K}(\Theta)=\Theta^{\lambda}\cdot\mathrm{K_{bkg}}\,, \ \text{with } \Theta\equiv\frac{\theta(z,t)-\theta_{res}}{\theta_{sat}(z,t)-\theta_{res}}\in[0,1]\,, \quad (5)$$

where $\lambda>0$ is a conceptual tunable parameter (not directly observed) and $\mathrm{K_{bkg}}$ has mean and variance given, respectively, by

$$\mathbb{E}[\mathrm{K_{bkg}}]=\mu(z) \quad \text{and} \quad \mathrm{Var}[\mathrm{K_{bkg}}]=\eta\cdot(1-\Theta)\,, \quad (6)$$

where $\mu(z)\geq 0\,\forall\, z\in[0,\ 20\ \mathrm{m}]$ is an exponentially decreasing function, and $\eta>0$.

The unique feature of this method is that at every depth and every time step, the variance changes inversely with the degree of saturation Θ, as a very simple representation of fracture flow. The density of the fractures is crudely represented by η. With full saturation ($\Theta=1$), the variance vanishes as water passes through all fractures, while it is greatest under dry conditions ($\Theta=0$), when multiple fractures are available for the passage of water.

Also, unlike studies that specify the porosity and saturated value of (K) at the soil surface and vary the *e*-folding distance, between 5 and 120 m, depending on slope [*Fan et al.*, 2007; *Maxwell and Miller*, 2005], *Vrettas and Fung* [2015] determines the exponentially decreasing profile of μ(z) using predefined values of the hydraulic conductivity (at saturation), at the top and bottom of the weathered bedrock. The hydraulic conductivity at saturation for soil, saprolite, and fresh bedrock are specified at 20, 7, and 0.5 [cm/h], respectively, and are the same as in *Vrettas and Fung* [2015].

After a large number of simulations that vary the values of λ and η, an optimal set of values was obtained that provided the best fit of the model response to the actual high-frequency fluctuations of the water table at seven wells over 6 years. For the purposes of this paper this set is fixed at $(\lambda=1, \eta=2)$.

2.3. Lateral (Subsurface) Flow

To capture the slow recessions of the water table between storms and during the dry months (as seen in *Vrettas and Fung* [2015, Figure 19]), it is necessary to include in the 1-D model an ad hoc term that mimics lateral flow. This is done by introducing a sink term, defined as follows:

$$\mathrm{LF}(z,\psi)=\begin{cases} -\gamma_{\mathrm{lat}}\cdot\psi(z,t), & z\in[z_{\hat{w}}, z_{\triangledown}] \\ 0, & \text{otherwise} \end{cases}, \tag{7}$$

where $z_{\hat{w}}$ is the simulated water table depth, $z_{\triangledown}$ is the observed water table, and $\gamma_{\mathrm{lat}}=2.5\cdot 10^{-4}\,[(\mathrm{LT})^{-1}]$ is a lateral conductivity parameter, chosen by trial and error to fit the recession at the location of interest. We note that this ad hoc procedure is effectively a "place-holder" for a more advanced model such as the TOPMODEL [*Niu et al*., 2005].

3. Root Distribution and Functioning

Knowledge of plant root characteristics such as depth, distribution, and functioning, is vital to improve modeling of the various hydrological processes and their effects on climate [*Feddes et al*., 2001]. CLM specifies rooting depths for each plant functional type (PFTs) and the profile of root fraction based on the extensive compilation of *Schenk and Jackson* [2002b]. These rooting depths vary between 1.5 and 3 m and the root fractions typically decrease exponentially with depth. However, observations in the tropics [*Nepstad et al*., 1994] show that these depths are conservative. There is no global or regional database on such plant traits, or roots that are deeper than 3 m. Inverse methods to infer rooting depths [*Kleidon*, 2004] yield insights into the geography of deep roots, but cannot be used to predict the evolution of roots in changing hydrologic regimes.

To focus on the sensitivity of transpiration to root structure and function, we prescribe a range of rooting profiles and calculate root uptake efficiency by implementing a combination of the algorithms of *Lai and Katul* [2000], modified by *Collins and Bras* [2007].

Root water uptake, interpreted as transpiration, is represented as a sink term (ET) in equation (1) and activated only during the daylight hours (defined here between 06:00 A.M. and 18:00 P.M.). We simplify this first approach by neglecting bare soil evaporation in the dense old-growth forest, and using the term ET (evapotranspiration) to refer to transpiration. Following *Feddes et al*. [2001], ET is represented as

$$\mathrm{ET}(\theta,z,t)=\mathrm{T}_{\mathrm{pot}}(t)\cdot r(z)\cdot\rho(\theta)\,, \tag{8}$$

where $\mathrm{T}_{\mathrm{pot}}(t)$ is potential transpiration, $r(z)$ is the root density at depth "z," and $\rho(\theta)$ is the root water uptake efficiency, as a function of soil moisture θ. Note that integrating equation (8), with respect to depth "z," will give the actual transpiration rate as

$$\mathrm{ET}_{\mathrm{act}}(t)=\int_0^{\mathrm{D}}\mathrm{ET}(z,t)dz\,, \tag{9}$$

where $\mathrm{D}>0$ is the maximum root depth and θ has been omitted for parsimony. Only under optimal water conditions will equation (9) be equal to the potential transpiration $\mathrm{T}_{\mathrm{pot}}(t)\;\forall\, t\geq 0$.

3.1. Root Density Profiles

Root density $r(z)$ is a dynamic system that depends, among other things, on climatic conditions and vegetation types [*Laio et al*., 2006; *Wijk and Bouten*, 2001], but is difficult to observe. In climate models, it is usually represented by simple analytic functions and is assumed to decrease with depth [*Gerwitz and Page*, 1974].

In this work we consider three different root density profiles given by (i) *Uniform*, (ii) *Gamma*, and (iii) *Negative Exponential* density functions. All profiles were defined between $z=0$ and $z=$ D, with $\mathrm{D}=\{3,5,8,10\}$ [m]. Note that since the actual densities are defined in either (-∞, +∞), or [0, +∞), the resulting profiles were normalized so that the condition: $\int_0^{\mathrm{D}} r(z)dz=1$, always holds true.

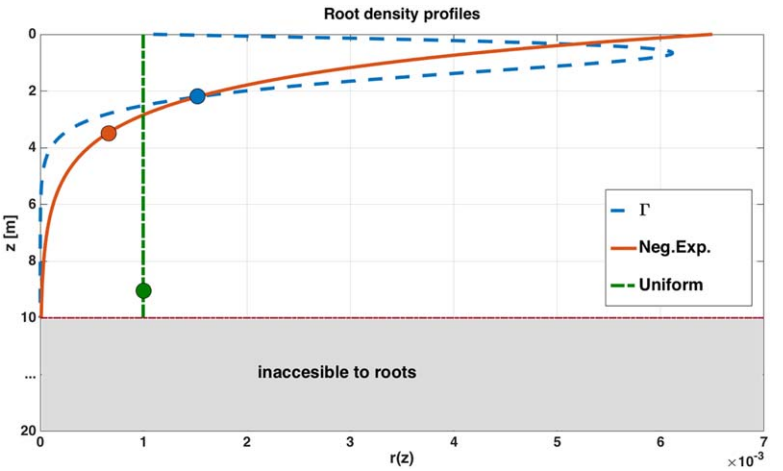

Figure 1. Root density profiles, as functions of depth z. In this example the maximum root depth is set to 10 m and the gray shaded area represents the depth that is inaccessible to the roots. The colored circles indicate the depth where each profile reaches 90% of root mass, from the surface ($z = 0$). Note that all functions are normalized so the area under the curve sums to one.

An example of the above densities is shown in Figure 1 for D = 10 m. With the exception of the uniform profile (dash-dotted green line), which does not have any tunable parameters, the other two profiles were parameterized to keep the majority of the mass above 3 m to stay close with the prescribed depths in the CLM [*Feddes et al*., 2001; *Lawrence et al*., 2011]. We note that 10% of the root mass is below 2, 3.5, and 9 m for the *Gamma*, *Negative Exponential*, and *Uniform* profiles, respectively.

3.2. Root Water Uptake Efficiency

Root water uptake efficiency models are usually empirical and do not allow a particular layer to extract more water than the potential transpiration that is given for this layer. This means that the lack of water at some depth cannot be compensated by the affluence of water in other layers inside the root-zone. In our approach we borrow ideas from *Collins and Bras* [2007] and use a root water uptake efficiency model that includes both local and bulk constraints for water uptake. The model compensates for the drier layers and extracts water from other more saturated cells, when the conditions allow it

$$\rho(\theta(z,t)) = \alpha_1(\theta(z,t)) \cdot \alpha_2(\theta(z,t)), \tag{10}$$

with the additional constraint of

$$\int_0^D \rho(\theta(z,t))dz \leq 1, \ \forall\, t \geq 0. \tag{11}$$

In equation (10) the maximum efficiency, when water is not limiting, is given by $\alpha_1(\cdot)$, such as

$$\alpha_1(\theta(z,t)) = \max\left\{\frac{\theta(z,t)}{\theta_{\text{sat}}(z)-\theta_{\text{wlt}}(z)}; \frac{\int_0^z \theta(z',t)dz'}{\int_0^D \theta(z',t)dz'}\right\}, \tag{12}$$

with the first expression in the $\max\{\cdot,\cdot\}$ representing the local effect, while the second the nonlocal compensating contribution. The root-shutdown is modeled by $\alpha_2(\cdot)$, as

$$\alpha_2(\theta(z,t)) = \begin{cases} 0, & \theta(z,t) \in [\theta_{\text{res}}, \theta_{\text{wlt}}(z)] \\ \dfrac{\theta(z,t)-\theta_{\text{wlt}}(z)}{\theta_{\text{fcp}}(z)-\theta_{\text{wlt}}(z)}, & \theta(z,t) \in (\theta_{\text{wlt}}(z), \theta_{\text{fcp}}(z)] \\ 1, & \theta(z,t) \in (\theta_{\text{fcp}}(z), \theta_{\text{sat}}(z)] \end{cases}, \tag{13}$$

and prevents the soil from drying out completely, below the predefined wilting point $\theta_{\text{wlt}}(z)$.

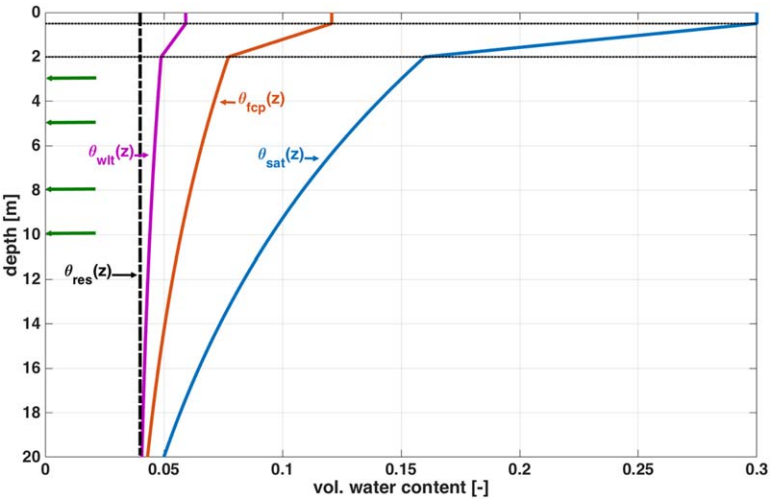

Figure 2. Schematic illustration of all the soil moisture profiles: $\theta_{res}(z)$, $\theta_{wlt}(z)$, $\theta_{fcp}(z)$, and $\theta_{sat}(z)$, as functions of depth. The horizontal black-dotted lines, near the surface, indicate the end of the soil and saprolite layers in the vertical domain. The green arrows locate the different rooting depths at 3, 5, 8, and 10 m, examined here.

Finally, there are two additional parameters in the above expressions, i.e., the wilting point $\theta_{wlt}(z)$ and field capacity $\theta_{fcp}(z)$, for which we have no observations. We define them as decreasing functions of depth using equation (2) as follows:

$$\theta_{fcp}(z) = \max\{\theta(\psi_{fcp}), \theta_{res}\}, \tag{14}$$

$$\theta_{wlt}(z) = \min\{\theta(\psi_{wlt}), \theta_{fcp}(z)\}, \tag{15}$$

with the matric potential values at field capacity and wilting point set to $\psi_{fcp} = 340$ cm ($\approx 1/3$ Bar) [*Nachabe*, 1998] and $\psi_{wlt} = -1500$ cm, respectively. An example of all the profiles used for the simulations in this article can be found in Figure 2.

It is clear that since we set an exponential decreasing function for the porosity $\theta_{sat}(z)$ (blue line), that will reflect also on the rest of the soil moisture parameters for the $\theta_{wlt}(z)$ and $\theta_{fcp}(z)$, making sure that the minimum value is always set above the residual water content at θ_{res}, which is kept constant with depth.

3.3. Hydraulic Redistribution

An important function of many root systems is hydraulic redistribution (HR), or hydraulic lift, the upward transport of water by the roots, usually during the night hours, from deeper soil layers to the upper soil layers, where the water can be extracted easily during the day by the dense roots [*Dawson*, 1993; *Burgess et al.*, 1998]. HR is directly observed by reversal of root sapflow [*Brooks et al.*, 2002; *Oliveira et al.*, 2005], as well as inferred from diurnal variations in ψ or θ between two depths in the upper 0.5−1.0 m of the soil column [*Dawson*, 1993; *Meinzer et al.*, 2004]. Here we do not explicitly model the downward transfer of water by tap roots and assume that the downward flux is driven by matric potential gradients in the soil and weathered bedrock.

Following *Lee et al.* [2006], $\mathrm{HR}(\psi, z)$ is modeled as a flux in equation (1) and is activated only during night hours (defined here between 18:00 P.M. and 06:00 A.M.). More specifically,

$$\mathrm{HR}(\psi, z) = -\mathrm{K}_{HR}(\psi, z) \cdot \Delta\psi(z, t), \tag{16}$$

where K_{HR} is the hydraulic conductance associated with HR, and $\Delta\psi$ is the difference in soil water potential between the uptake and release layers in the soil profile. As in *Lee et al.* [2006], K_{HR} is given by

$$\mathrm{K}_{HR}(\psi, z) = A \cdot LAI \cdot (1 + \psi/\psi_{50})^2 \cdot r(z), \tag{17}$$

where $A = 0.5 \cdot 10^{-3}$ [kg/s MPa^{-1}], *LAI* is the leaf area index, ψ_{50} is the water potential at 50% saturation of the discrete cell, and $r(z)$ is the normalized root density at depth "z." As light attenuates in the tree canopy, we set LAI equal to 4, which is smaller than the actual leaf area index, to mimic a light-weighted average.

4. Model Experiments

To investigate how subsurface characteristics influence the magnitude and seasonality of ET in a Mediterranean climate, we carried out a series of experiments with the 1-D model described above. The experiments vary (1) annual precipitation amount; (2) annual ET demand; (3) ET demand seasonality; (4) rooting profile; (5) rooting depth; and (6) inclusion of hydraulic redistribution. An additional experiment reduced the hydraulic conductivity K by 50%, to represent a different lithological setting with slower infiltration. These are described below.

For the experiments, we consider a "reference" year (WY2008), a "wet" year (WY2010), and a "dry" year (WY2013), with annual precipitation of 1500, 2100, and 1000 mm, respectively. Winter precipitation comprises ∼85% of annual precipitation during the reference and wet years, and ∼70% during the dry year. The "control" experiment is the case from *Vrettas and Fung* [2015], with precipitation for the reference year and no ET.

To explore how ET of different tree species could be sustained in the region, we specify the annual ET demands and their partitioning between the wet and dry seasons. We include cases with annual ET demands that are 10, 20, 30, 40, and 50% of WY2008 annual precipitation minus interception, assumed to be fixed at 10% of annual precipitation. For simplicity, we shall refer to these cases as annual ET demands of 135, 270, 405, 540, and 675 mm/a.

The timing of ET varies with tree species, as well as with precipitation, temperature, VPD, and other aspects of weather and climate. At Rivendell, a strong dependence of sapflow velocities on insolation and VPD was found [*Link et al*., 2014], so that sapflow velocities integrated over the wet winters (October–March) are typically lower than that for dry summers (April–September). We consider three hypothetical partitionings of the annual ET between the wet and dry seasons: "wet deciduous" tree cover with 100% ET in the wet season, a combination of wet deciduous and Mediterranean vegetation (50%), and Mediterranean vegetation with 30% of the annual ET demand in the wet season. We recognize, for example, that wet deciduous trees are found in the wet tropics and are not common in this winter-rain region. We include them for completeness, and for exploring the maximum ET that could be realized when the seasons of precipitation and ET are synchronous. For each case, the total ET demand for each season is partitioned uniformly among the daytime hours (between 06:00 A.M. and 18:00 P.M. local time) within the season, thus ignoring day-to-day and hour-to-hour variations. This neglect should not impact the inventory of subsurface moisture, which integrates over the high-frequency variations in precipitation input and outputs via ET and runoff.

Lacking any information about the rooting structure or root functioning of the trees at the site, we varied several root properties whose combinations could be interpreted to represent the functioning of a wide range of plant species. These traits include rooting profile (uniform, gamma, and negative exponential), maximum rooting depth (3, 5, 8, and 10 m), and presence/absence of hydraulic redistribution (HR).

We did not detect hydraulic redistribution in the limited number of tree roots instrumented with sapflow sensors. However, *Meinzer et al*. [2004] inferred HR by Douglas-firs from the observation that near-surface soils in the vicinity of Douglas-firs were wetter at night than in the daytime. In a small watershed with a dense forest cover and intertwining tree roots, we assume that HR by Douglas-firs would benefit all vegetation in their vicinity. The HR-noHR experiments could thus be interpreted as the ET response of a tree species with a particular root depth in the absence or presence of Douglas-firs nearby. For each case, the 1-D model was integrated forward in time, for a complete water year.

5. Results

The vertical distribution of soil and rock moisture $\theta(z,t)$ typically follows the porosity profile and decreases with depth. In a region with weathered bedrock, the profile of effective saturation $\Theta(z,t)$ in the control case (no ET) is the opposite, with the highest degree of saturation above the water table, where preferential flow readily saturates the region with low porosity, further facilitating faster flow (Figure 3a). In the annual mean, about 30% of the moisture in the column is in the thick layer of weathered bedrock between 3 and 20 m.

Root extraction of moisture leads to reduced hydraulic conductivity in the root zone (equation (5)) compared to the control (no ET), resulting in slightly less penetration of moisture to the weathered bedrock

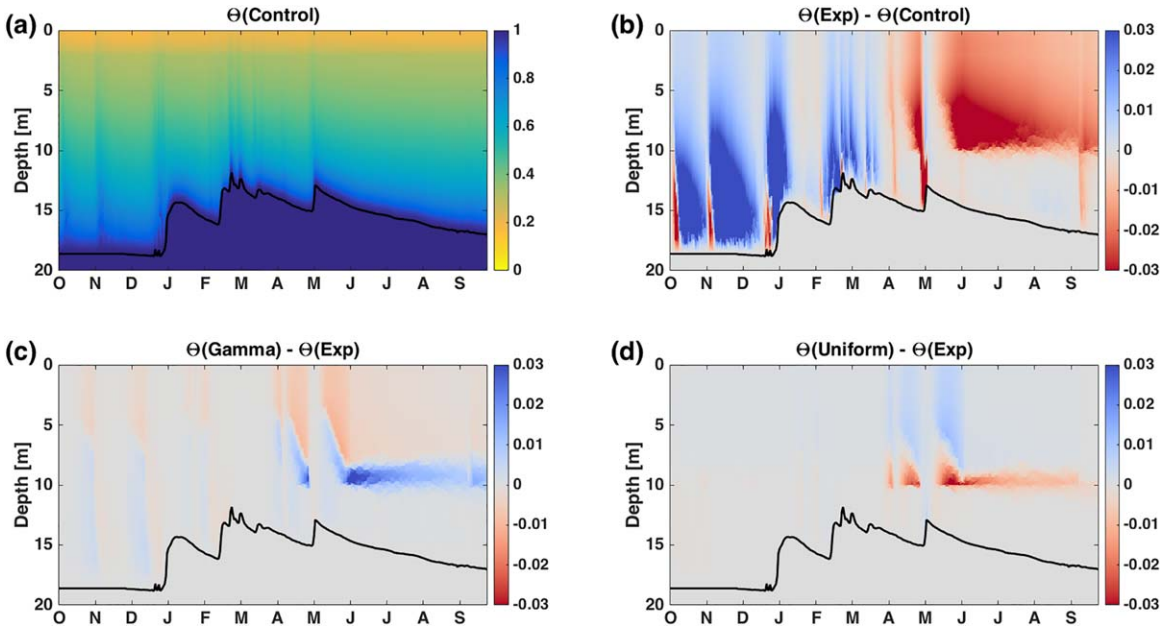

Figure 3. Evolution of (a) normalized soil and rock moisture Θ, for the control case without ET, and of (b) $\Delta\Theta_{exp}$, the moisture departure from the control case. (c) The difference in Θ between the case with gamma root profile and negative exponential root profile. (d) Same as Figure 3c, but for uniform root profile. The setting for these results is WY2008, D = 10 m, ET demand of 675 mm/a, partitioned 30:70 between the wet and dry seasons. The black solid line shows the observed water table depth, as a function of time.

below, especially after winter rains. This is shown in Figure 3b, for the case with a negative exponential root profile extending to D = 10 m, annual rainfall of 1000 mm/a, and an annual ET demand of 675 mm/a partitioned 30:70 between the wet and dry seasons. During the dry season, the saturation difference, $\Delta\Theta_{exp}=\Theta_{exp}-\Theta_{control}$, shows an interesting pattern that reflects the combined effect of the vertical profiles of root density, porosity, and wilting point. Moisture extraction is greatest from the upper ∼3 m where $r(z)$ is large. The extraction slows when θ_{exp} approaches the wilting point θ_{wlt}, which has the highest values in the upper soils, and so $\Delta\Theta_{exp}$ is less negative than at the beginning of the dry season. Between ∼3 m and D = 10 m, even though the extraction is smaller than in the upper soils, θ_{wlt} and θ_{sat} decrease rapidly with depth (Figure 2), and so $\Delta\Theta_{exp}$ is more negative than in the upper soils.

Because the three root profiles are normalized to have the same root mass, the resulting profiles of moisture extraction follow, to lowest order, the root density profiles. Hence, compared to Θ_{exp}, Θ_{gamma} is lower in the upper parts of the soil column and higher around 10 m (Figure 3c). Similarly, the moisture differences between $\Theta_{uniform}$ and Θ_{exp} follow the $r(z)$ difference (Figure 3d). The actual annual ET is highest for the case where there is the greatest root density at depth, i.e., the uniform profile, but the difference is small, ∼1%.

In the following, we focus on the negative exponential rooting profile. Table 1 shows, for the three water years, the actual annual ET for the experiments with different ET demands and rooting depths. The discussion below will highlight several systematics that emerge from the results.

The case of the hypothetical wet deciduous vegetation illustrates the maximum ET that could be attained in the rainy winter, when the demand is less than the precipitation input. Figure 4 shows modeled ET for wet deciduous vegetation (100% of the ET demand in the wet winter) for the reference year and the dry year, for the range of ET demands and rooting depths. For the reference year, the actual ET matches the ET demand only when the demand is very low (<300 mm/a) (Figure 4a). With high ET demand (675 mm/a), actual ET is 70−80% of that demand even with roots at 8 or 10 m. The situation is exacerbated in the dry year (2013–2014), when the maximum actual ET is less than half the demand for all maximum root depths (Figure 4b). Not surprisingly, shifting the ET demand progressively to the dry summer decreases the actual annual ET (Table 1). For the case with a demand of 675 mm/a partitioned 70% in the dry summer, the actual ET is lower, by more than 100 mm/a, than that of "wet deciduous vegetation" for all rooting depths for the reference and wet years.

Table 1. Actual Annual ET (mm/a) for Different Precipitation (mm/a), ET Demand (mm/a), and Maximum Root Depth D (m)[a]

		Maximum Root Depth D											
		3 m			5 m			8 m			10 m		
Precip.	ET	100:0	50:50	30:70	100:0	50:50	30:70	100:0	50:50	30:70	100:0	50:50	30:70
1000 (mm)	135	63	57	52	81	76	67	109	110	93	124	120	102
	270	110	101	93	134	129	116	170	173	156	188	198	170
	405	145	139	120	178	173	155	221	222	203	243	251	225
	540	171	167	140	211	209	181	265	264	238	290	296	265
	675	196	189	158	240	238	202	304	302	265	333	336	295
1500 (mm)	135	115	94	93	127	113	108	133	131	120	134	134	130
	270	203	167	153	223	190	176	251	223	192	268	247	207
	405	270	220	196	298	255	224	337	294	254	370	324	271
	540	325	259	234	365	300	265	411	360	311	449	393	334
	675	371	293	264	423	339	303	479	417	358	520	460	394
2100 (mm)	135	122	104	96	128	120	108	134	129	118	134	134	126
	270	234	197	170	247	216	191	257	233	205	266	242	215
	405	328	278	231	350	303	258	376	327	283	386	342	294
	540	409	349	287	442	383	318	485	414	355	505	434	369
	675	485	412	338	524	455	374	580	498	418	609	519	440

[a]The seasonality of ET demand (wet:dry) is reported in percentages. The experiments used negative exponential root profiles, the standard stochastic hydraulic conductivity, and no hydraulic redistribution.

In the following, we focus on the cases where the annual ET demand of 675 mm/a is partitioned 30:70 between the wet and dry seasons, as there is abundant sunlight and higher vapor pressure deficit in the summer. In these cases, summer ET demand exceeds summer precipitation, and so summer ET must rely on residual soil and rock moisture at the end of the winter rains.

The ET realized during the wet and dry seasons for different maximum root depths and annual precipitation is shown in Figure 5. As would be expected, actual annual ET increases with annual precipitation and with rooting depth. In the reference and wet years when winter precipitation input exceeds the winter demand

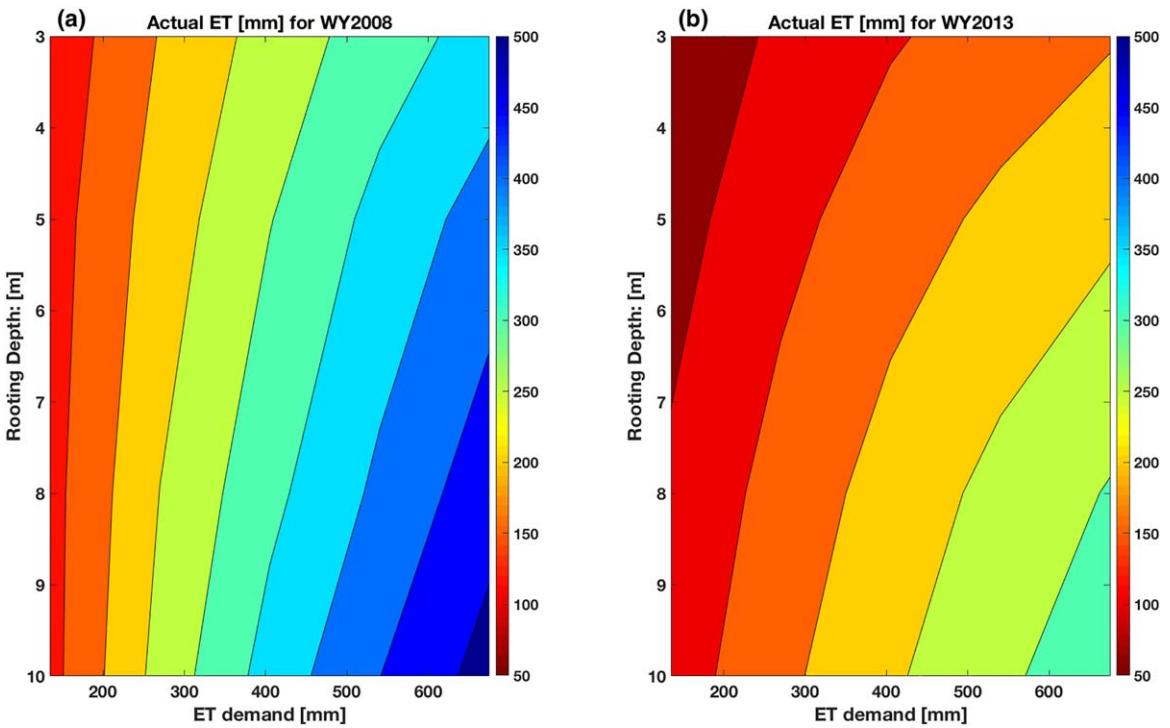

Figure 4. Sensitivity of actual annual ET to different moisture demands and rooting depths. All cases have annual precipitation for WY2008 and WY2013 of 1500 and 1000 mm/a, respectively, and 100% of the ET demand is in the wet winter. Unit is mm/a.

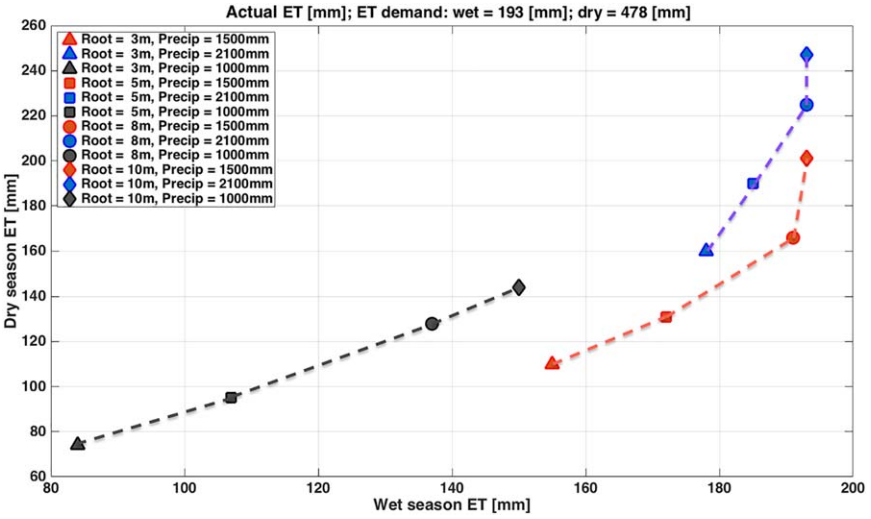

Figure 5. Partitioning of actual ET [mm/a] between the wet and dry seasons for different annual precipitation amounts (colors) and different maximum root depths D (symbols). The black, red, and blue symbols are for cases with annual precipitation of 1000, 1500, and 2100 mm/a, respectively. The dashed lines connect actual ET for D = 3, 5, 8, and 10 m.

by more than fivefold, wet season ET reaches the demand only with D > 8 m. In the dry year, winter precipitation input still exceeds the winter demand by a factor of 3. Yet the maximum actual winter ET, for D = 10 m, is only ∼75% of the demand, as heavy rains facilitate faster transit of water to below the root zone. The actual dry season ET is largest when D increases from 8 to 10 m, as the deep roots can access residual moisture at the end of the rainy season, but still cannot reach the demand. In this region with rapid infiltration, there is not enough moisture in the upper soil and saprolite layers to support high ET by vegetation with shallow roots.

Figure 6 shows the influence of HR on wet and dry season ET for a maximum root depth of 10 m and for the 3 years. HR is impactful in the dry seasons or in a dry year, when the competition between the rates of precipitation input and infiltration leaves behind a sufficient amount of water in the root zone. With the K derived for the conductive subsurface in this region, HR-enhancement of annual ET is ∼40 mm/a, and is largest, though by only a small amount, in the reference year, as there is low input during the dry year, and fast transit during the wet year. HR-enhancement during the wet season is negligible, except for the dry year. In the cases with halved K, there is greater retention of moisture in the root zone, and the dry season

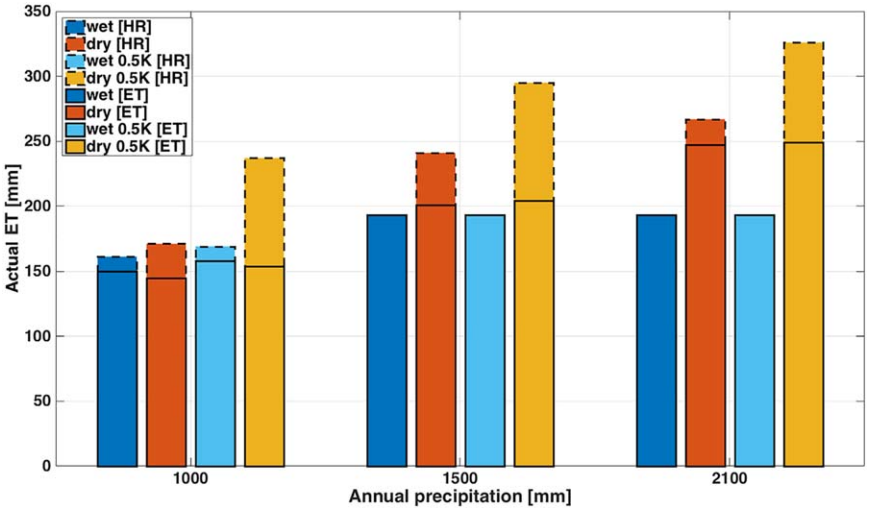

Figure 6. Impact of HR (highlighted with the dashed lines) on wet and dry season ET for annual precipitation amounts of 1000, 1500, and 2100 mm/a, from the experiments with D = 10 m, ET demand of 675 mm/a, partitioned 30:70 between the wet and dry seasons.

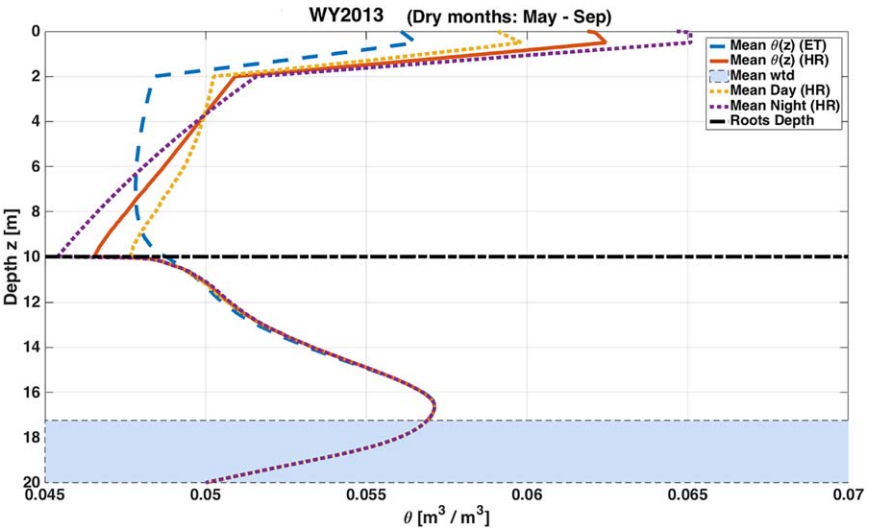

Figure 7. Diurnal variations of soil and rock moisture $\theta(z)$ m^3/m^3 averaged over the dry season, from the experiment with annual precipitation of 1000 mm/a (WY2013), 10 m roots, ET demand of 675 mm/a, partitioned 30:70 between the wet and dry seasons. The shaded light blue denotes the water table averaged over May–September 2014.

HR-enhancements, relative to the standard K cases, are increased further by 66, 53, and 58 mm/a, for the dry, reference, and wet years, respectively. In the wet season, when the hydraulic conductivity is high, the HR-enhancement is negligible, except for less than 10 mm/a for the dry year.

Hydraulic redistribution typically occurs at night when roots transfer water from depth to the near-surface to support ET. Figure 7 shows the diurnal variations in $\theta(z)$ for the dry season of the dry year (WY2013), when HR is most effective. As is expected from *Dawson* [1993], inclusion of HR yields near-surface moisture that is higher at night than daytime, and the reverse in the weathered bedrock. The diurnal variation of $\theta(z)$ in the soil layer is $\sim$0.005. The diurnal variation is not obtained without HR (not shown). Averaged over the dry season, HR impact on $\theta(z)$ is an increase of $\sim$0.005 near the surface. The $\theta(z)$ maximum at $\sim$17 m separates the saturated zone below from the vadose zone above (cf. $\theta_{sat}(z)$ in Figure 2), and is equivalent to the effective saturation Θ shown in Figure 3a.

The effect of hydraulic conductivity (K) on annual ET is shown in Figure 8a, for a combination of annual precipitation and rooting depths. The annual ET demand is 675 mm/a, 70% of which is in the dry season. As discussed above, ET with HR increases with precipitation and with rooting depth. Even with 10 m roots and HR, the maximum annual ET achieved is $\sim$330 mm/a during the dry year, $\sim$49% of the demand. With halved K, there is an enhancement in ET for all precipitation and rooting depths (Figure 8b), as there is slower transit of moisture to below the root zone. The enhancement is greatest for deep-rooted systems during the dry year, and is as large as 50$-$70 mm/a.

There is a negative, albeit small, feedback in the deep root zone: depletion of moisture by ET (especially with HR) decreases hydraulic conductivity and enhances the retention of moisture. In this way, even though the magnitude of the actual ET (with HR) increases with annual precipitation, ET expressed as a percentage of annual precipitation decreases slightly with increasing precipitation (32, 29, and 22% for the dry, reference, and wet years, respectively) for the case with 10 m roots and annual ET demand of 675 mm/a. In this model with preferential flow, the corresponding actual ET percentages for the case with the same demand but 3 m roots are practically indistinguishable (16, 18, and 16%, respectively).

The resultant annually averaged trend in storage is close to zero (–70 to + 63 mm/a) for all rooting depths and ET demands (not shown). The negative storage trends are found for wet years, when the infiltration is fast, as well as for dry years, when recharge is diminished.

6. Discussion and Summary

It is a truism that the amount of moisture transpired by vegetation is critically tied to the moisture supply accessible to the root system. At a small, steep hillslope in Northern California, multiyear high-frequency

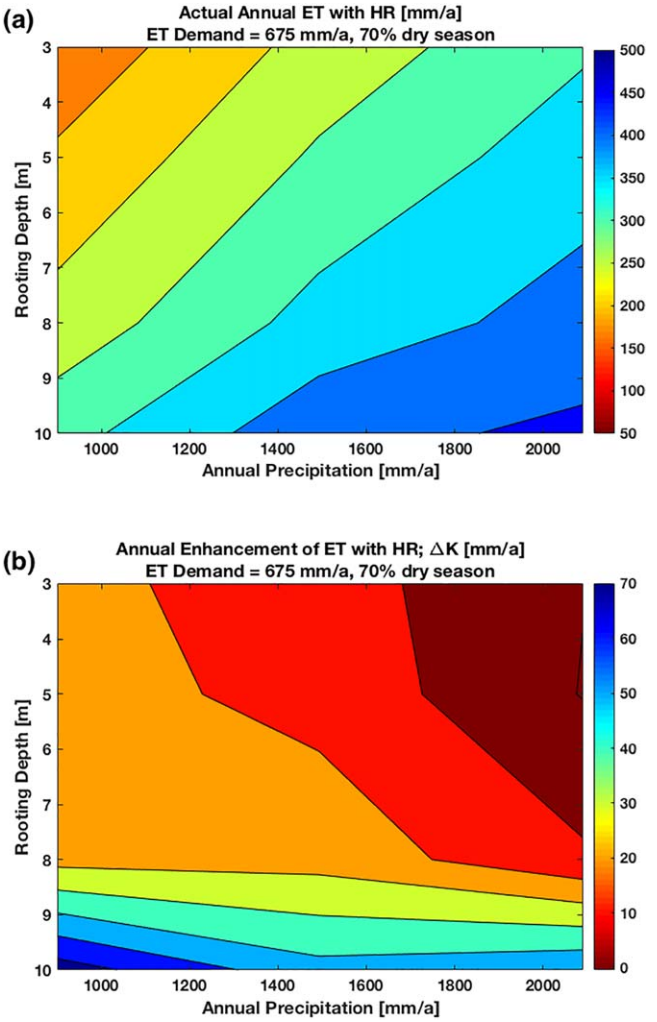

Figure 8. (a) Actual annual ET (with HR) for different maximum root depths and annual precipitation amounts. (b) Enhancement of ET, relative to Figure 8a, when hydraulic conductivity is reduced by 50%. Results are from experiments with exponential root profiles, ET demand of 675 mm/a, partitioned 30:70 between the wet and dry seasons. Unit is mm/a.

observations of maximal sapflow velocities in some trees during the dry summers raise the question about the dynamics of the moisture in the root zone and about how the trees access the moisture. Furthermore, the water table in multiple wells shows rapid rise and slow decline after rainstorms, suggesting significant preferential flow through macropores and fractures. We model the preferential flow using Richards' equation with a new stochastic parameterization of hydraulic conductivity whose mean value increases, but whose variance decreases, with saturation [*Vrettas and Fung*, 2015]. Furthermore, the profile of saturated hydraulic conductivity is determined by the thickness of the weathered bedrock and the conductivity at the top of the weathered bedrock. The ad hoc parameterization of lateral flow in the 1-D model is a "place-holder" for more sophisticated treatments.

This study extends *Vrettas and Fung* [2015] and presents a series of model experiments that explore how ET of different trees in a Mediterranean climate is influenced by their root properties, where a significant portion of the ET is observed to take place in the dry and sunny summer when the precipitation is insufficient to meet the demand. In the experiments, we varied annual maximum ET demand, seasonality of the demand, as well as rooting depths in an attempt to represent the ET and root distribution of different tree species. We also included or excluded hydraulic redistribution by roots, and included a special case when we investigated the sensitivity of ET in a less permeable substrate. We have not explicitly included evaporation from bare soil in this first study, as it would have little impact on moisture profiles below a few centimeters.

From the results, we ask: given a tree species whose ET magnitude and seasonality are known approximately, what root characteristics are needed to survive in this precipitation and geologic setting? We find that actual ET in a Mediterranean climate nearly doubles when the maximum rooting depth is increased from 3 to 10 m. For trees with 10 m roots, it is the roots below 4 m, comprising 10% of the root mass, that access moisture in the weathered bedrock to sustain summer ET. For the 3 years we investigated with annual precipitation ranging between 1000 and 2100 mm/a, both ET and lateral subsurface runoff (LF) increase with increasing precipitation. However, the ET fraction of precipitation decreases with increasing precipitation, as hydraulic conductivity increases with Θ. Consistent with field observations [*Brooks et al.*, 2006], our results show that hydraulic redistribution is important for sustaining ET in the dry seasons when the vertical gradient in water potential ($\partial\psi/\partial z$) is large. The relative ET enhancement is $\sim$20% in the reference year, and less (around 10%) in a rainy year, when there is rapid transit and less retention of moisture in the root zone.

The maximum annual actual ET for our experiments is ~460 mm/a, for the case where the prescribed demand is 675 mm/a, partitioned 30:70 between wet:dry seasons, with 10 m roots, and HR contributing ~ 40 mm/a in the dry season. This estimate is comparable to the value of 500 mm/a we infer from the intercept of the discharge-rainfall relationship for the entire Eel River watershed with an area of ~9500 km^2 [*Syvitski and Morehead*, 1999]. Halving the hydraulic conductivity, as would be done for further downstream where there is a thicker soil mantle and different lithology, could increase the ET as much as 60 mm/a in a dry year, with most of the increase from HR.

The results highlight the importance of lithology, species composition, and root function for ET, especially under dry conditions. Where there are fractures in the weathered bedrock and likely soil and rock moisture, we would expect roots deep enough to access the moisture, and hydraulic redistribution to be most effective. The species composition and associated plant traits are manifested in the seasonality of ET: our observations show that different evergreen trees have very different sap velocity response to precipitation. The maximum ET realized for a region thus depends on the optimal combination of precipitation, plant traits, and subsurface conditions: too much precipitation in a region with a highly fractured subsurface would promote infiltration and runoff at the expense of storage, and greater wet-season ET demand would deplete moisture store for the summer.

We thus hypothesize that lithology, in addition to climate, is an important factor in the distribution of vegetation and that trees that survive prolonged droughts have deep roots and are found in regions with weathered bedrock which may be a nonnegligible inventory of water. Indeed in Northern California, there is a clear demarcation between evergreen forests along the coast and deciduous woodlands some 10 km inland. The demarcation outlines different geologic formations resulting from the subduction of the Pacific-Farallon plate under North America. With the same rainstorm, overland flow is observed inland and not in the Coastal Belt, exposing their different permeabilities and water storage capacities.

The study presented here is a first step and prototypes an approach toward understanding resilience of vegetation to droughts. A dynamic root model may be coupled to carbon allocation models already implemented in CESMs. Implementation of the framework presented here into global climate models is encouraged by recent progress in several directions. These include (1) a global gridded data set of the thicknesses (up to 50 m) of soil, weathered bedrock, and sedimentary deposits [*Pelletier et al*., 2016], (2) inference of effective hydraulic conductivity and fracture density in the weathered bedrock from high-frequency observations of the water table [*Vrettas and Fung*, 2015], (3) inference of ecosystems that utilize groundwater [*Thompson et al*., 2011; *Pérez Hoyos et al*., 2016]. Also, model results can be cross-checked by satellite observations, such as skin (top 5 cm) moisture from SMAP data, in areas other than dense forests where vegetation water content exceeds 5 kg/m^2 [*Entekhabi et al*., 2010], and by the column-integral of water loading from GRACE [*Tapley et al*., 2004]. Advancing the modeling and constraining model results will require characterization of decreasing exponentials for porosity, wilting point, and field capacity, as well as high-frequency vertical profiles of subsurface moisture, extending to a depth of 10 m or more.

Notation

ITCZ	intertropical convergence zone.
C4MIP	coupled carbon cycle climate model intercomparison project.
IPCC	intergovernmental panel on climate change.
DGVM	dynamic global vegetation model.
HR	hydraulic redistribution.
CLM	community land model.
ET	evapotranspiration.
CESM	community earth system model.
WY	water year.
PFT	plant functional type.
SMAP	soil moisture active passive.
GRACE	gravity recovery and climate experiment.

Acknowledgments
This work was funded by the NSF Mathematics and Climate Research Network (DMS-0940272), NSF Critical Zone Observatory (EAR-1331940), and the Department of Energy (DE-SC0010857 and DE-SC0014080). Inez Fung was partially supported by a University of California Agricultural Experiment Station grant. The data sets used in this paper were collected as part of the Berkeley HydroWatch project supported by the W. M. Keck Foundation. To inquire about accessing the data, please visit http://sensor.berkeley.edu.

References

Arora, V., et al. (2013), Carbon-concentration and carbon-climate feedbacks in CMIP5 earth system models, *J. Clim.*, *26*, 5289–5314, doi:10.1175/JCLI-D-12-00494.1.
Asner, G. P., P. G. Brodrick, C. B. Anderson, N. Vaughn, D. E. Knapp, and R. E. Martin (2016), Progressive forest canopy water loss during the 2012-2015 California drought, *Proc. Natl. Acad. Sci. U. S. A.*, *113*(2), E249–E255, doi:10.1073/pnas.1523397113.
Band, L. E., et al. (2014), Ecohydrological flow networks in the subsurface, *Ecohydrology*, *7*, 1073–1078.
Beven, K., and P. Germann (2013), Macropores and water flow in soils revisited, *Water Resour. Res.*, *49*, 3071–3092, doi:10.1002/wrcr.20156.
Brooks, J., F. Meinzer, R. Coulombe, and J. Gregg (2002), Hydraulic redistribution of soil water during summer drought in two contrasting pacific northwest coniferous forests, *Tree Physiol.*, *22*, 1107–1117.
Brooks, J., F. Meinzer, J. Warren, J.-C. Domec, and R. Coulombe (2006), Hydraulic redistribution in a Douglas-fir forest: Lessons from system manipulations, *Plant Cell Environ.*, *29*, 138–150.
Brooks, R. H., and A. T. Corey (1964), Hydraulic Properties of Porous Media, Hydrol. Pap., vol. *3*, 27 pp., Colo. State Univ., Fort Collins.
Burgess, S., N. Adams, N. Turner, and C. Ong (1998), The redistribution of soil water by tree root systems, *Oecologia*, *115*, 306–311.
Collins, D. B. G., and R. L. Bras (2007), Plant rooting strategies in water limited ecosystems, *Water Resour. Res.*, *43*, W06407, doi:10.1029/2006WR005541.
Cox, P., R. A. Betts, C. D. Jones, S. A. Spall, and I. J. Totterdell (2000), Acceleration of global warming due to carbon-cycle feedbacks in a coupled climate model, *Nature*, *408*, 184–187, doi:10.1038/35041539.
Dawson, T. E. (1993), Hydraulic lift and water use by plants: implications for water balance, performance and plant–plant interactions, *Oecologia*, *95*, 565–574.
Entekhabi, D., et al. (2010), The soil moisture active passive (SMAP) mission, in Proc. IEEE, *98*, 704–716, doi:10.1109/JPROC.2010.2043918.
Fan, Y., G. Miguez-Macho, C. P. Weaver, R. Walko, and A. Robock (2007), Incorporating water table dynamics in climate modeling: 1. Water table observations and equilibrium water table simulations, *J. Geophys. Res.*, *112*, D10125, doi:10.1029/2006JD008111.
Feddes, R. A., et al. (2001), Modeling root water uptake in hydrological and climate models, *Bull. Am. Meteorol. Soc.*, *82*(12), 2797–2809.
Friedlingstein, P., et al. (2006), Climate-carbon cycle feedback analysis: Results from the C4MIP model intercomparison, *J. Clim.*, *19*, 3337–3353.
Fung, I. Y., S. C. Doney, K. Lindsay, and J. John (2005), Evolution of carbon sinks in a changing climate, *Proc. Natl. Acad. Sci. U. S. A.*, *102*(32), 11,201–11,206.
Gardner, W. R. (1957), Some steady-state solutions of the unsaturated moisture flow equation with application to evapotranspiration from a water table, *Soil Sci. Soc. Am.*, *85*, 228–232.
Gerwitz, A., and E. R. Page (1974), An empirical mathematical model to describe plant root systems, *J. Appl. Ecol.*, *11*(2), 773–781.
Jackson, R. B., L. A. Moore, W. A. Hoffmann, W. T. Pockman, and C. R. Linder (1999), Ecosystem rooting depth determined with caves and DNA, *Proc. Natl. Acad. Sci. U. S. A.*, *96*, 11,387–11,392.
Kharin, V. V., F. W. Zwiers, X. Zhang, and M. Wehner (2013), Changes in temperature and precipitation extremes in the CMIP5 ensemble, *Clim. Change*, *119*(2), 345–357, doi:10.1007/s10584-013-0705-8.
Kleidon, A. (2004), Global datasets of rooting zone depth inferred from inverse methods, *J. Clim.*, *17*, 2714–2722.
Lai, C.-T., and G. Katul (2000), The dynamic role of root-water uptake in coupling potential to actual transpiration, *Adv. Water Resour.*, *23*, 427–439.
Laio, F., P. D'Odorico, and L. Ridolfi (2006), An analytical model to relate the vertical root distribution to climate and soil properties, *Geophys. Res. Lett.*, *33*, L18401, doi:10.1029/2006GL027331.
Lawrence, D. M., et al. (2011), Parameterization improvements and functional and structural advances in version 4 of the community land model, *J. Adv. Model. Earth Syst.*, *3*, M03001, doi:10.1029/2011MS00045.
Lee, J.-E., R. S. Oliveira, T. E. Dawson, and I. Fung (2006), Root functioning modifies seasonal climate, *Proc. Natl. Acad. Sci. U. S. A.*, *102*, 17,576–17,581.
Leung, L. R., M. Huang, Y. Qian, and X. Liang (2011), Climate-soil-vegetation control on groundwater table dynamics and its feedbacks in a climate model, *Clim. Dyn.*, *36*, 57–81, doi:10.1007/s00382-010-0746-x.
Link, P., K. Simonin, H. Maness, J. Oshun, T. Dawson, and I. Fung (2014), Species differences in the seasonality of evergreen tree transpiration in a Mediterranean climate: Analysis of multiyear, half-hourly sap flow observations, *Water Resour. Res.*, *50*, 1869–1894, doi:10.1002/2013WR014023.
Maxwell, R. M., and N. L. Miller (2005), Development of a coupled land surface and groundwater model, *J. Hydrometeorol.*, *6*, 233–247.
Meinzer, F., J. Brooks, S. Bucci, G. Goldstein, F. Scholz, and J. Warren (2004), Converging patterns of uptake and hydraulic redistribution of soil water in contrasting woody vegetation types, *Tree Physiol.*, *24*(8), 919–928.
Miralles, D. G., J. H. Gash, T. R. Holmes, R. A. de Jeu, and A. J. Dolman (2010), Global canopy interception from satellite observations, *J. Geophys. Res.*, *115*, D16122, doi:10.1029/2009JD013530.
Nachabe, M. H. (1998), Refining the definition of field capacity in the literature, *J. Irrig. Drain. Eng.*, *124*, 230–232.
Nepstad, D. C., C. De Carvalho, E. Davidson, P. Jipp, P. Lefebvre, G. Negreiros, E. Da Silva, T. Stone, S. Trumbore, and S. Vieira (1994), The role of deep roots in the hydrological and carbon cycles of Amazonian forests and pastures, *Nature*, *372*, 666–669.
Niu, G.-Y., Z.-L. Yang, R. E. Dickinson, and L. E. Gulden (2005), A simple TOPMODEL-based runoff parameterization (SIMTOP) for use in global climate models, *J. Geophys. Res.*, *110*, D21106, doi:10.1029/2005JD006111.
Oleson, K. W., et al. (2013), Technical description of version 4.5 of the community land model (CLM), *NCAR Tech. Note NCAR/TN-503+STR*, Natl. Cent. for Atmos. Res., Boulder, Colo.
Oliveira, R. S., T. E. Dawson, S. S. Burgess, and D. C. Nepstad (2005), Hydraulic redistribution in three Amazonian trees, *Oecologia*, *145*, 354–363.
Pelletier, J., P. Broxton, P. Hazenberg, X. Zeng, P. Troch, G.-Y. Niu, Z. Williams, M. Brunke, and D. Gochis (2016), A gridded global data set of soil, immobile regolith, and sedimentary deposit thicknesses for regional and global land surface modeling, *J. Adv. Model. Earth Syst.*, *8*, 41–65, doi:10.1002/2015MS000526.
Pérez Hoyos, I. C., N. Y. Krakauer, and R. Khanbilvardi (2016), Estimating the probability of vegetation to be groundwater dependent based on the evaluation of tree models, *Environments*, *3*, 1–21, doi:10.3390/environments3020009.
Poot, P., and H. Lambers (2008), Shallow-soil endemics: Adaptive advantages and constraints of a specialized root-system morphology, *New Phytol.*, *178*, 371–381, doi:10.1111/j.1469-8137.2007.02370.x.
Salve, R., D. M. Rempe, and W. E. Dietrich (2012), Rain, rock moisture dynamics, and the rapid response of perched groundwater in weathered, fractured argillite underlying a steep hill-slope, *Water Resour. Res.*, *48*, W11528, doi:10.1029/2012WR012583.

Schenk, H. J. (2008), Soil depth, plant rooting strategies and species' niches, *New Phytol.*, *178*, 223–225.
Schenk, H. J., and R. B. Jackson (2002a), The global biogeography of roots, *Ecol. Monogr.*, *72*(3), 311–328.
Schenk, H. J., and R. B. Jackson (2002b), Rooting depths, lateral root spreads and below-ground/above-ground allometries of plants in water-limited ecosystems, *J. Ecol.*, *90*, 480–494.
Schwinning, S. (2010), The ecohydrology of roots in rocks, *Ecohydrology*, *3*, 238–245.
Scoccimarro, E., S. Gualdi, A. Bellucci, M. Zampieri, and A. Navarra (2013), Heavy precipitation events in a warmer climate: Results from CMIP5 models, *J. Clim.*, *26*, 7902–7911, doi:10.1175/JCLI-D-12-00850.1.
Sillmann, J., V. V. Kharin, X. Zhang, F. W. Zwiers, and D. Bronaugh (2013a), Climate extremes indices in the CMIP5 multimodel ensemble: Part 1. Model evaluation in the present climate, *J. Geophys. Res. Atmos.*, *118*, 1716–1733, doi:10.1002/jgrd.50203.
Sillmann, J., V. V. Kharin, F. W. Zwiers, X. Zhang, and D. Bronaugh (2013b), Climate extremes indices in the CMIP5 multimodel ensemble: 2. Future climate projections, *J. Geophys. Res. Atmos.*, *118*, 2473–2493, doi:10.1002/jgrd.50188.
Swann, A. L., I. Fung, and J. Chiang (2012), Mid-latitude afforestation shifts general circulation and tropical precipitation, *Proc. Natl. Acad. Sci. U. S. A.*, *109*, 712–716, doi:10.1073/pnas.1116706108.
Syvitski, J. P., and M. D. Morehead (1999), Estimating river-sediment discharge to the ocean: Application to the Eel margin, northern California, *Mar. Geol.*, *154*, 13–28.
Tang, J., W. Riley, and J. Niu (2015), Incorporating root hydraulic redistribution in CLM4.5: Effects on predicted site and global evapotranspiration, soil moisture, and water storage, *J. Adv. Model. Earth Syst.*, *7*(4), 1828–1848.
Tapley, B., S. Bettadpur, J. Ries, P. F. Thompson, and M. M. Watkins (2004), GRACE measurements of mass variability in the Earth system, *Science*, *305*(5683), 503–505.
Teuling, A., et al. (2010), Contrasting response of European forest and grassland energy exchange to heatwaves, *Nat. Geosci.*, *3*, 722–727, doi:10.1038/NGEO950.
Thompson, S., C. Harman, A. Konings, M. Sivapalan, A. Neal, and P. Troch (2011), Comparative hydrology across AmeriFlux sites: The variable roles of climate, vegetation, and groundwater, *Water Resour. Res.*, *47*, W00J07, doi:10.1029/2010WR009797.
van Genuchten, M. T. (1980), A closed-form equation for predicting the hydraulic conductivity of unsaturated soils, *Soil Sci. Soc. Am.*, *44*(5), 1–8.
van Genuchten, M. T., and D. R. Nielsen (1985), On describing and predicting the hydraulic properties of unsaturated soils, *Ann. Geophys.*, *3*(5), 615–628.
van der Molen, M. K., et al. (2011), Drought and ecosystem carbon cycling, *Agric. For. Meteorol.*, *151*, 765–773.
Vrettas, M. D., and I. Y. Fung (2015), Toward a new parameterization of hydraulic conductivity in climate models: Simulation of rapid groundwater fluctuations in Northern California, *J. Adv. Model. Earth Syst.*, *7*, 2105–2135, doi:10.1002/2015MS000516.
Wijk, M. T. V., and W. Bouten (2001), Towards understanding tree root profiles: Simulating hydrologically optimal strategies for root distribution, *Hydrol. Earth Syst. Sci.*, *5*(4), 629–644.
Zwieniecki, M. A., and M. Newton (1996), Seasonal pattern of water depletion from soil-rock profiles in a Mediterranean climate in southwestern Oregon, *Can. J. For. Res.*, *26*(8), 1346–1352.